What is the Ground-State Structure of the Thinnest Si Nanowires?

Yufeng Zhao and Boris I. Yakobson*

*Department of Mechanical Engineering and Material Science, and Department of Chemistry, Rice University,
Houston, Texas 77005, USA*

Pristine silicon whiskers are compared through energy analysis by separating the surface, edge, and bulk contributions, and by energy computation for a variety of structures and diameters d. It is shown that for $d < 6$ nm a polycrystalline wire of five-fold symmetry, rather than single-crystal types, represents the ground state. It remains stable in molecular dynamics tests up to ~ 1000 K. Its specific surface reconstruction also stands out in that it favors kinetics of whisker growth and thus appears potentially realizable.

Highly anisotropic needlelike crystals (whiskers) have long been a subject of physics and materials science. This interest, especially in the ultimately thin varieties, has been recently stimulated by the potential need for interconnects and wires in nanoelectronics [1–5]. It has been further heightened by the discovery of nanotubes [6] that demonstrated structural stability of subnanometer thick solids. Nanotubes differ qualitatively from other whiskers in that their "bulk" crystal structure (with the Bravais lattice and primitive cell as its attributes) is essentially absent while the surface is completely homogeneous. This permits their cylindrical shape. In contrast, the first problem one faces for a bulk-based whisker is to determine its cross-section shape. For a given thickness (that is, a number N of atoms in a cross section of diameter $d \sim N^{1/2}$) what shape corresponds to the lowest energy and is likely to be more stable? For macroscopic solids ($N \rightarrow \infty$) Wulff construction provides a classical recipe [7], relating equilibrium shape with the surface energies γ_s of different facets. It solves the energy minimization problem of $\min \sum s\gamma_s$ at $N = $ const (surface being measured by a number s of appropriate unit cells). In this approach the energy of the edges E_e ($\sim d^0 \sim N^0$) between the facets is neglected compared to the surface contribution ($\sim s \sim d \sim N^{1/2}$), while the bulk ($\sim d^2 \sim N$) is assumed already at its minimum and thus invariant. For nanometer thickness, N can be as small as a few dozens, and therefore the Wulff energy must be augmented,

$$F = E_e + s\gamma_s + E_b, \qquad (1)$$

to include the energy of matching the adjacent facets E_e. It can affect their surface reconstruction [8] and even favor certain changes in the bulk as reflected by E_b (including possibly internal granularity or elastic strain, if such would lower the energy overall).

Although several possible pristine Si nanowire (SiNW) structures [4,8–10] have previously been discussed, no basis for comparison has been developed. Equation (1) provides such a starting point for evaluating different structures and possibly selecting the ground state.

According to Eq. (1), it may be favorable at the nanoscale to abandon a usual perfection of the bulk in order to achieve low-energy matching at the edges. Figure 1(a) shows the Si-lattice structure projected to the (110) plane. The optimal design comes from a prism cut along the [110] direction in bulk Si with a (100) and two {111} planes forming a nearly $2\pi/5$ angle, $\theta = 2\tan^{-1}(1/\sqrt{2})$, with $\varepsilon = \theta - 2\pi/5 = 0.025$. Therefore, with little shear
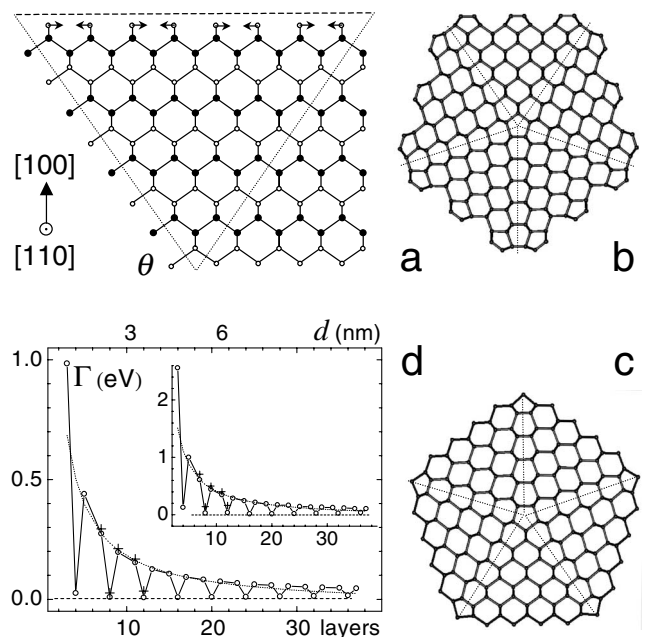

FIG. 1. (a) Si lattice viewed along the [110] axis shows the dark and light atoms displaced by $a/2$ in the axial direction, so that the slanted off-plane bonds appear shorter than the in-plane bonds; arrows indicate dimerization of surface atoms. Five prisms outlined by the triangle can join in pentagonal wire with the surface dimer rows either parallel (b) or perpendicular (c) to the wire axis; shown are 12-layer thick $P_\parallel$ and 11-layer thick $P_\perp$. (d) Energy dependence on nanowire thickness computed with classical EP (circles) and TB (crosses). The inverse-linear curve (dotted) is fitted to the sample points at 7 and 17 layers. The inset is for carbon.

strain ε and inexpensive {111} stacking faults, five such prisms can form a pentagonal rod P, where all (100) facets permit low-energy reconstruction with characteristic dimer-row pattern. The (100) surface cell has a size a equal to the second nearest neighbor distance in the bulk and used hereafter as a length unit ($a = 3.84$ Å for Si and 2.52 Å for C).

The alignment of the dimer rows is known to alternate between two orthogonal directions when the bulk lattice grows in consecutive layers [11]. The degeneracy of these row patterns is lifted since their orientation with respect to the wire becomes important. Surface dimerization in the wires of $4l$ atomic layers follows the arrows in Fig. 1(a), with dimer rows parallel to this $P_{\parallel}$ wire, Fig. 1(b). For $(2l-1)$ layers the circumferential dimer rows run perpendicular to the $P_{\perp}$ wire, Fig. 1(c). The $2(2l-1)$ layer wires are not permissible because of a surface atom column left unpaired in each facet.

A comparison of $P_{\parallel}$ and $P_{\perp}$ rods can be performed by direct computations with many-body empirical potentials (EP) [12,13], in order to illustrate the significance of the edge-energies and also to validate the heuristically useful but approximate decomposition (1). With the E_b term including in this case the energies of stacking fault [14] $s\gamma_f$ and of bulk shear [15] strain $\frac{1}{2}NK\varepsilon^2$, Eq. (1) yields $F - s\gamma_s = E_e + s\gamma_f + \frac{1}{2}NK\varepsilon^2$, where s is counted as a number of three-fold coordinated atoms (one per surface cell). For convenience of comparison, the *excess surface energy*, $\Gamma = (F - s\gamma_s)/s$, is plotted in Fig. 1(d) versus number of atomic layers. The deduction of a large trivial contribution $s\gamma_s$ reduces the error in absolute value of surface energies computed with different methods. It is clearly seen that the computed points corresponding to $P_{\parallel}$ and $P_{\perp}$ fit, respectively, to a horizontal line (dashed line, $\Gamma = 0$) and an inverse-linear curve (dotted line, $\Gamma \sim 1/d$), indicating the overwhelming edge-energy over the almost negligible stacking fault and elastic energy corrections.

The inset of Fig. 1(d) plots Γ for isomorphic C wires, similar to the case of Si, in spite of different interatomic forces. This again demonstrates the robustness of Eq. (1). Since the surface-counting method (s as a number of three-fold coordinated atoms) is identical for $P_{\parallel}$ and $P_{\perp}$, Fig. 1(d) can be interpreted as evidence of very low edge-energy in $P_{\parallel}$, at least in comparison with the $P_{\perp}$ series. This originates from their structures, Figs. 1(b) and 1(c): little strain is added to the edges of $P_{\parallel}$, while the $P_{\perp}$ wire is rather strained in the corner pentagons. (Putting in one more atomic column to change the pentagon into a hexagon places the steps on both sides of the edge, which raises the energy.)

For series of rather large systems (up to 10^4 atoms in the computation cell, $4a$ in length) and to reveal general dependencies, EP [12,13] are used to faster compute the energies. They are also used below in molecular dynamics (MD) tests. Further, when only sample wires are needed

for evaluating parameters in Eq. (1), they are computed using tight-binding approximation [16] (TB). Bulk, (100)-(2×1) surface and wire structures were calculated with 3D, 2D, and 1D periodic boundary conditions, respectively, with the box periods optimized.

In the following we extend a comparison of the $P_{\parallel}$ wires with others of hexagonal (H) and square (S) shapes, as most feasible 1D structures. Indeed, since both the (100) and (111) surfaces have the lowest energies [17,18], a competitive family is the hexagonal bars with these facets, sized according to Wulff's theorem, that is, equilateral. The (100) facets with axially aligned dimer rows match the {111} facets in Fig. 2(b): two of the {111} facets follow the normal π-bond chain model [19] while the other two have incomplete reconstruction leaving two rows of atoms similar to an unreconstructed surface.
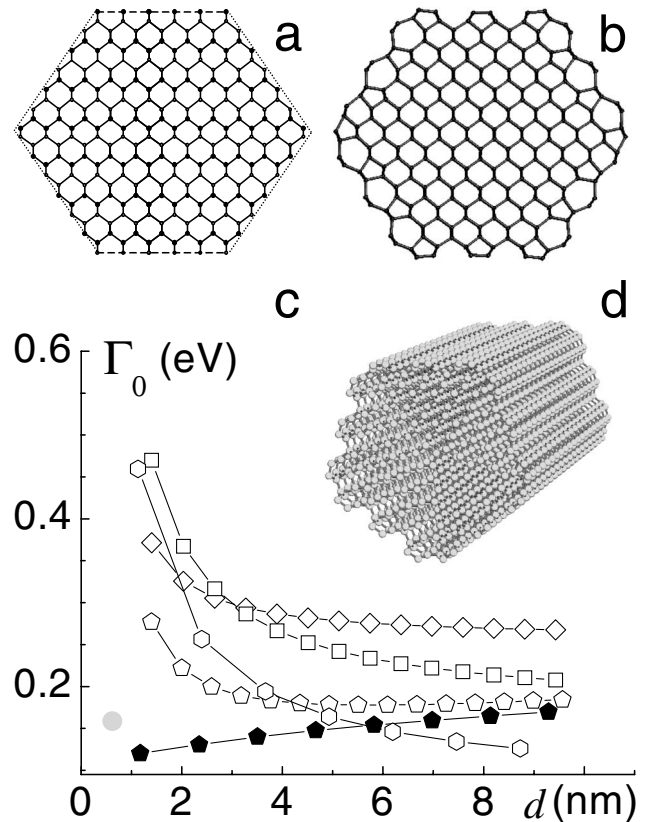

FIG. 2.   Hexagonal wire with four {111} and two {100} unreconstructed (a) and reconstructed (b) facets. Size-dependent energy (c) of different types of wires obtained as extrapolation based on several sample-point large-scale computations. The lowest energy line (solid pentagons) makes the ground state for $d < 6$ nm evident as $P_{\parallel}$ structure, shown in (d). Added here for completeness, $P_{\perp}$ plot (open pentagons) differs from $P_{\parallel}$ due to significant edge-energy, $E_e = 4.3$ eV. Curves with open hexagons, squares, and diamonds denote, respectively, H, $S_{\square}$, and $S_{\diamond}$ wires. The shaded circle corresponds to the chain of fullerenelike Si_{20} clusters, whose energy is the lowest among this variety; see Fig. 5(c) in Ref. [4].

S bars cut out by four {100} planes have been discussed [8] with two possible reconstructions, i.e., (2×1) [or $p(2 \times 2)$] and $c(2 \times 2)$ denoted here as $S_\square$ and $S_\diamond$, according to the reconstruction patterns.

Comparison between the $S_\square$, $S_\diamond$, H, and $P_\parallel$ should be based on their energies $F(N)$, whose direct computation is, however, not practical given the numerous (a hundred) structures of interest and the large size (up to $\sim 10^4$ atoms) of each. Equation (1), reduced to $F = E_e + s\gamma_s$ for the monocrystalline S and H bars, offers an economical way. First we define a method to count s, evaluate the corresponding $E_e = F - s\gamma_s$ from computed sample structures, and find E_e to be almost invariant within the isomorphic families. Then the free energies for the whole group are evaluated as $F = E_e + s\gamma_s$ without repetitive full computations. Indeed, the number of cross-sectional atoms N and the surface area s are explicitly counted and given in Table I. Obtained from TB computations edge-energies E_e agree with the estimates [20] based on *ab initio* data.

On the other hand, we find that our TB computations underestimate the stacking fault γ_f and strain energy (although TB results are higher than EP). Therefore, for conservative comparison [21] of $P_\parallel$ with other wires in Fig. 2(c), we use the TB-computed E_e's and *ab initio* surface energies; for the $P_\parallel$ family, we use *ab initio* computed stacking fault [14] $\gamma_f = 0.06$ eV and experiment-based shear modulus, $K = 48$ GPa $= 5.9$ eV/atom for Si in the corresponding direction [15].

Table I can be readily used for energy evaluation at arbitrary size. By generalizing the Γ plot in Fig. 1(d), we plot now $\Gamma_0 = (F - s_0\gamma_0)/s_0$ as a function of the effective diameter d, Fig. 2(c). Here $\gamma_0 = 1.32$ eV per a^2 area is the surface energy [17,18] of Si(100)-(2×1) or (111)-(2×1), and the effective surface area $s_0 = 2.11N^{1/2}$ corresponds to the cylinder of diameter d, containing N atoms.

Obtained with the decomposition-extrapolation (1) approach, Fig. 2(c) represents well the energies of the wires; for example, the asymptotic levels at $d \rightarrow \infty$ correspond to their relative shape-determined surface areas (lowest for the H and highest for the S types) or surface energies. Notably, the curves here also reproduce more subtle features, such as a crossover point for the two types of square S bars, obtained in large scale computation [8]. Not surprisingly, for the smallest range $d < 1.5$ nm decomposition (1) shows its limitations, as the strain overlap between the edges makes the energy higher than simple addition. Direct calculation for the $P_\parallel$ of $d = 1.1$ nm yields energy almost as high as that of one fullerene cluster wire in Fig. 2(c), while all the thicker SiNW results fall well on the line. The energies for other cluster chains [4,5,9,10] are yet higher due to dangling bonds and/or substantial strain, if H terminated [5].

Turning to the ground state issue, it is useful to corroborate the evidence of Fig. 2(c) with an estimate. In the spirit of analysis [20], for all the whiskers here, the edge-energy is roughly 1 eV (dangling bond energy) per edge or 4–5 eV total. (The apparent edge-energy for H is lower because the extra density of dangling bonds at the edges is contained in s.) The $P_\parallel$ wire is unique in its edge reconstruction almost indistinguishable from the facets and thus $E_e = 0$; instead there is a cost of the stacking fault and elastic shear, $(0.06s + 0.002N)$ eV. It will surpass the edge-energy only for s and N at about 20 layers, i.e., $d \sim 6$ nm , while a $3 \sim 4$ nm $P_\parallel$ wire remains well below its competitors in energy.

To further verify stability, we perform a MD test for ~ 1 ns at $T = 1000$ K. Figure 3 shows that after 10 ps C wires gradually transform into the tubelike patterns, while Si wires remain stable. At much longer times capillary instability should not be neglected [22].

Besides the lower energy, the $P_\parallel$ structures also kinetically favor the whisker growth due to highly anisotropic diffusion of adatoms on the Si(100)-(2×1) surface. It is about 1000 times faster along the flat dimer rows than across the row-groove corrugation [23]. On the surface of a $P_\perp$, circumferential diffusion facilitates an accretion of the next layer, transforming it into a $P_\parallel$ type. (Such thickness growth may be accompanied by shape oscillations [24], which is beyond the scope of the present report; we simply emphasize the kinetic advantages of the $P_\parallel$ wires for unidirectional growth.) At $T = 550$ K, diffusion rate [23] $D = 10^{-9}$ cm^2 s^{-1}, and deposition rate of less than 0.015 MLs^{-1} (monolayer, 1 ML $= 1/a^2$), an adatom propagates along a 1 μm wire faster to the ends than an ad dimer or an island can emerge. Even a dimer vacancy, which often occurs on the normal (100)-(2×1) surface, is more likely to migrate to this whisker's end [25]. This kinetics favors a $P_\parallel$ structure. In contrast, all other wires do not support such an enhanced axial diffusion.

The above analysis of both energy and kinetics, together with experimental evidence [4] suggests that high-vacuum growth of SiNW offers an efficient practical way complementary to vapor-liquid-solid growth [2]. Pristine SiNW must be passivated prior to any use in ambient
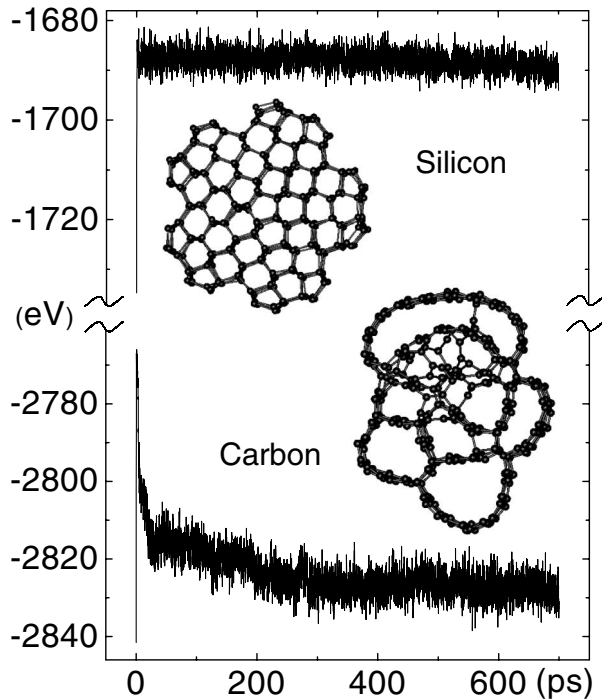
TABLE I. Parameters (measured per length of a) used to calculate energy of SiNW: $l = 1, 2, 3, \ldots, N$ is the number of all atoms, s is a number of surface atoms. The surface energy $\gamma_0 = 1.32$ eV for (100)- and (111)-(2×1) is based on Ref. [18], while that of $c(2 \times 2)$ relative to 2×1 is based on Ref. [8]. The area $\sqrt{3}a^2/2$ per (111) surface atom is used to define s for the H bars.

	N	s	E_e	$\gamma_s - \gamma_0$
$S_\square$	$(8l^2 + 12l + 1)/\sqrt{2}$	$8l/\sqrt{2}$	5.58	0
$S_\diamond$	$(8l^2 + 12l + 1)/\sqrt{2}$	$8l/\sqrt{2}$	3.56	0.077
H	$4l(6l + 1)$	$2l(2 + 2\sqrt{3})$	1.96	0
$P_\parallel$	$10l(2l + 1)$	$10l$	0	0

FIG. 3. Potential energy and structural changes of eight-layer $P_\parallel$ wires in MD simulations at $T = 1000$ K. The insets show the final structures of relatively stable Si (top) and of C transforming into sp^2 tubular-graphitic foam (bottom).

environment. Energy comparison for passivated wires can still be based on Eq. (1), but with additional terms $-\sum \mu_p s_p$ accounting for the chemical potentials μ_p and numbers s_p of the passivating groups (index p being H, O, OH, etc.). The results depend on conditions (μ_p), and the details go far beyond the scope of the current report. Moreover, when passivation follows the growth, it effectively seals the wire as it was grown.

In summary, we have compared several families of SiNWs and singled out a very stable type. With lower ground state energy, reasonable thermal stability, and surface kinetics favorable for axial growth, these nanowires appear to be promising 1D pristine silicon structures. Small SiNWs have been reported [26] after the submission of this manuscript. These wires, obtained by acid thinning of a bulk-structured Si core, could not be of the P family; the H type is the next in the energy range [Figs. 2(a)–2(c)] and is consistent with the reported hexagonal shape with four {111} and two {100} facets [26].

———————————

*Corresponding author: biy@rice.edu

[1] D. Appell, Nature (London) **419**, 553 (2002).

[2] A. M. Morales and C. M. Lieber, Science **279**, 208 (1998); Y. Huang *et al.*, *ibid.* **294**, 1313 (2001).

[3] Y. F. Zhang *et al.*, Appl. Phys. Lett. **72**, 1835 (1998).

[4] B. Marsen and K. Sattler, Phys. Rev. B **60**, 11 593 (1999).

[5] U. Landman *et al.*, Phys. Rev. Lett. **85**, 1958 (2000).

[6] S. Iijima, Nature (London) **354**, 56 (1991); N. G. Chopra *et al.*, Science **269**, 966 (1995).

[7] C. Herring, Phys. Rev. **82**, 87 (1951).

[8] S. Ismail-Beigi and T. Arias, Phys. Rev. B **57**, 11 923 (1999).

[9] M. Menon and E. Richter, Phys. Rev. Lett. **83**, 792 (1999).

[10] B.-X. Li *et al.*, Phys. Rev. B **65**, 125305 (2002).

[11] D. J. Chadi, Phys. Rev. Lett. **59**, 1691 (1987).

[12] J. Tersoff, Phys. Rev. B **38**, 9902 (1988).

[13] D. W. Brenner, Phys. Rev. B **42**, 9458 (1990).

[14] D. Vanderbilt, Phys. Rev. Lett. **59**, 1456 (1987). Note that the number of surface atoms in P-type nanowires equals that of atoms at the interface; therefore, γ_f is stacking-fault energy per interface atoms which is known as 0.06 eV for silicon.

[15] J. J. Wortman and R. A. Evans, J. Appl. Phys. **36**, 153 (1965).

[16] C. Z. Wang, B. C. Pan, and K. M. Ho, J. Phys. Condens. Matter **11**, 2043 (1999).

[17] The complex (111)-(7×7) reconstruction is not considered because the matching at edges would lead to complicated defects with many dangling bonds. See Y. F. Zhao *et al.*, J. Vac. Sci. Technol. A **18**, 320 (2000).

[18] A. A. Stekolnikov, J. Furthmuller, and F. Bechstedt, Phys. Rev. B **65**, 115318 (2002).

[19] K. C. Pandey, Phys. Rev. Lett. **47**, 1913 (1981); **49**, 223 (1982).

[20] Energy modeling of complex surface based on simpler surfaces has proved to be successful, see D. Vanderbilt, Phys. Rev. B **36**, 6209 (1987); G-X. Qian and D. J. Chadi, J. Vac. Sci. Technol. B **4**, 1079 (1986). For example, in each edge of $S_\diamond$, there is a three-coordinated atom in a length of $\sqrt{2}a$. This edge atom is not a standard (100) surface atom, hence, it was not counted in s. Its formation energy from the bulk is the surface energy of the relaxed (111) per surface atom (1.37 eV); therefore, $E_e = 4 \times 1.37/\sqrt{2} = 3.88$ eV.

[21] Alternatively, all parameters can be obtained from only TB computations of several sample energies $F(N)$ and then solving coupled linear algebraic equations within each family to determine the edge, surface, etc., energy parameters. This leads to a series of plots similar to Fig. 2(d) but with even greater gap between $P_\parallel$ and other nanowires.

[22] D. J. Srolovitz and S. A. Safran, J. Appl. Phys. **60**, 255 (1986).

[23] Y. W. Mo, J. Kleiner, M. B. Webb, and M. G. Lagally, Phys. Rev. Lett. **66**, 1998 (1991).

[24] J. Tersoff, A. W. Denier van der Gon, and R. M. Tromp, Phys. Rev. Lett. **70**, 1143 (1993).

[25] Z. Zhang, H. Chen, B. C. Bolding, and M. G. Lagally, Phys. Rev. Lett. **71**, 3677 (1993).

[26] D. D. D. Ma *et al.*, Science **299**, 1874 (2003).